

## Computational materials discovery for lanthanide hydrides at high pressure for high temperature superconductivity

Evgeny Plekhanov<sup>✉,\*</sup>, Zelong Zhao<sup>✉</sup>, Francesco Macheda, Yao Wei<sup>✉</sup>, Nicola Bonini,<sup>†</sup> and Cedric Weber<sup>‡</sup>  
*Theory and Simulation of Condensed Matter (TSCM), King's College London, The Strand, London WC2R 2LS, United Kingdom*

 (Received 31 August 2021; revised 7 January 2022; accepted 11 January 2022; published 31 March 2022)

Hydrogen-rich superhydrides are believed to be very promising high critical temperature (high  $T_c$ ) superconductors, with experimentally observed critical temperatures near room temperature, as shown in recently discovered lanthanide superhydrides at very high pressures, e.g., LaH<sub>10</sub> at 170 GPa and CeH<sub>9</sub> at 150 GPa. With the motivation of discovering new hydrogen-rich high  $T_c$  superconductors at the lowest possible pressure, quantitative theoretical predictions are needed. In these promising compounds, superconductivity is mediated by the highly energetic lattice vibrations associated with hydrogen and their interplay with the electronic structure, requiring fine descriptions of the electronic properties, notoriously challenging for correlated  $f$  systems. In this paper, we propose a first-principles calculation platform with the inclusion of many-body corrections to evaluate the detailed physical properties of the Ce-H system and to understand the structure, stability, and superconductivity of CeH<sub>9</sub> at high pressure. We report how the calculation of  $T_c$  is affected by the hierarchy of many-body corrections and obtain a compelling increase in  $T_c$  at the highest level of theory, which goes in the direction of experimental observations. Our findings shed significant light on the search for superhydrides in close similarity with atomic hydrogen within a feasible pressure range. We provide a practical platform to further investigate and understand conventional superconductivity in hydrogen-rich superhydrides.

DOI: [10.1103/PhysRevResearch.4.013248](https://doi.org/10.1103/PhysRevResearch.4.013248)

### I. INTRODUCTION

Pressure, like temperature, is a basic thermodynamic quantity which can be applied in experiments over an enormous range, leading to important contributions in such diverse areas of science and technology as astrophysics, geophysics, condensed matter physics, chemistry, and biology [1]. Pressure can lead to a variety of new phenomena, a striking example being alkali metals, which exhibit a series of electronic phase transitions to superconducting [2], complex structural forms that might lack periodicity [3], and peculiar optical reflectivity [4], when compressed even modestly.

In particular, the search for superconducting metallic hydrogen at very high pressures has long been viewed as a key problem in physics [4] and is not new. Ashcroft proposed very early that hydrogen-based materials containing other main group atoms might exhibit superconductivity at large temperature [5]. These considerations are based on the Bardeen-Cooper-Schrieffer (BCS) theory, where superconductivity is phonon mediated, and has motivated many theoretical and experimental efforts in the search for high

temperature superconductivity in hydrides at high pressures [6]. A recent milestone has been achieved with (near-)room-temperature superconductivity in hydrogen disulfide [7,8].

Hydrogen disulfide has not previously been considered as a superconductor because it was believed to go through dissociation at high pressure. Recent theoretical work [9] indicated, however, that the dissociation would not occur, and Li *et al.* predicted that the material would become superconducting at  $1.6 \times 10^6$  atm, with temperatures above 80 K. This led to the practical experimental work of Drozdov *et al.* [7], who compressed the hydrogen disulfide in a diamond anvil cell. Theoretical calculations predicted that hydrogen sulfide would transform on compression to a superconductor with a  $T_c$  up to 200 K [9]. The high critical temperature  $T_c$  of 203 K at 150 GPa in samples formed by compression of H<sub>2</sub>S was subsequently confirmed [10].

This discovery has motivated scientists to expand further the scope of research to lanthanide hydrides under pressure, such as La-H [11] and Y-H [9]. For the La-H systems, remarkably, not only the  $d$  electrons of La and  $s$  electrons of H contribute to the Fermi density and hence to superconductivity, but also the  $f$  electrons of the lanthanide.

Interestingly, density functional theory (DFT) calculations have shown that the fcc LaH<sub>10</sub> is a good metal with several bands crossing the Fermi level along many directions, associated with a large electronic density at the Fermi level [12]. It was suggested that the contribution of  $f$  states is dominant, realizing a unique high  $T_c$  with  $f$  electrons at the Fermi level, in sharp contrast with the YH<sub>10</sub> system, where only the  $d$  electrons of Y and  $s$  electrons of H are the main contributors to Fermi density at high pressures [13]. This is due to

\*Corresponding author: [evgeny.plekhanov@kcl.ac.uk](mailto:evgeny.plekhanov@kcl.ac.uk)

†Corresponding author: [nicola.bonini@kcl.ac.uk](mailto:nicola.bonini@kcl.ac.uk)

‡Corresponding author: [cedric.weber@kcl.ac.uk](mailto:cedric.weber@kcl.ac.uk)

the fact that external pressure destabilizes La 6s and La 5d orbitals to a greater extent than the La 4f orbital, which populates upon pressure. This opens new exciting avenues into the prediction and design of novel superconductors at high pressure, which would involve *f* electrons, notoriously difficult to model in DFT, due to the strong electronic correlation effects.

Indeed, the effects of electron localization and hybridization are applicable to all high-density matter but are in particular relevant for the large family of correlated materials, based on transition metal *d* or lanthanide and rare-earth *f* elements. Correlated systems show a breadth of peculiar and interesting properties stemming from many-body effects, such as high temperature superconductivity in copper oxides and room-temperature metal-insulator transition in vanadates. A fair understanding has been obtained, in particular, with the Zaanen-Sawatzky-Allen (ZSA) theory [14], which provides a classification of transition metal periodic solids in terms of charge transfer or Mott systems, but the understanding of their properties far from ambient conditions remains lacking and challenging.

Hence, with the motivation of discovering new hydrogen-rich high  $T_c$  superconductors at the lowest possible pressure, quantitative theoretical predictions are needed. In these promising compounds, superconductivity is mediated by the interaction between the highly energetic lattice vibrations of hydrogen and electrons, requiring fine descriptions of the electronic properties, notoriously challenging for correlated *f* systems. Electronic correlations provide corrections for several theoretical elements, in particular, the electron-phonon coupling strength  $\lambda$ , the phonon-dispersion relations, the electron spectral weight, and cross terms between electron-electron and electron-phonon interactions.

As many-body corrections to phonon-dispersion relations are generally less dramatic than corrections to spectral functions (see, for instance, Ref. [15]), and their full treatment is beyond reach, we propose in this paper a pragmatic first-principles calculation platform which provides many-body corrections for the electronic spectral weight, which in turn provides corrected estimates of  $\lambda$  and superconducting temperatures. Indeed, many-body corrections in *f* systems can induce dramatic changes, with energy shifts on the scale of 1 eV or more, albeit with a systematic improvement obtained by dynamical mean-field theory (DMFT) as observed in metal-oxygen in actinides and rare-earth oxides [16]. We evaluate here the detailed physical properties of the Ce-H system, and we focus, in particular, on the effect of spectral transfer induced by electronic correlations [17,18].

CeH<sub>9</sub> crystallizes in a  $P6_3/mmc$  clathrate structure with a very dense three-dimensional atomic hydrogen sublattice at 100 GPa. We report how the calculation of  $T_c$  is affected by the hierarchy of many-body corrections and obtain a remarkable agreement at the highest level of theory. Our findings shed significant light on the search for superhydrides in close similarity with atomic hydrogen within a feasible pressure range. We provide a practical platform to further investigate and understand conventional superconductivity in hydrogen-rich superhydrides.

## II. DISCUSSION

The idea that hydrogen-rich compounds may be potential high  $T_c$  superconductors has originated from the beginning of the millennium, when chemical precompression was proposed as an effective way to reduce the metallization pressure of hydrogen by the presence of other elements, leading to observed  $T_c$  exceeding 200 K in the LaH<sub>10</sub> system [19] and 130 K in CeH<sub>9</sub> [20], which has indicated compressed hydrogen-rich compounds as potential room-temperature superconductors.

It is recognized that superconductivity in such hydrides owes its origin to electron-phonon coupling. According to BCS theory,  $T_c$  is mainly determined by four parameters: the characteristic phonon frequency, the electron-phonon coupling strength, the density of states at the Fermi level, and the  $\mu^*$ . It is widely accepted that density functional theory with standard pseudopotentials, such as the Perdew-Burke-Ernzerhof (PBE) functional, provides an accurate description of the lattice dynamics. However, DFT notoriously struggles with the treatment of strong electronic correlations for compounds with weakly hybridized and localized *f* electrons, such as Ce, where many-body corrections are called for. In this paper, we use the density functional theory approach extended with DMFT. DMFT readily provides corrections associated with the charge and spin local fluctuations, relevant, in particular, for the local paramagnetic moment of lanthanide elements. Typically, DMFT accounts for changes in orbital character at the Fermi surface, due to spectral weight transfer associated with the splitting of Hubbard *f* bands. As described in Methods, this affects, in turn, low energy electron-electron scattering processes via phonon momentum transfer, as captured by the Allen-Dynes formalism. We focus hereafter on the CeH<sub>9</sub>  $P6_3/mmc$  system at 200 GPa.

Firstly, we explore the effects of the many-body corrections at various levels of theory (see Fig. 1). We observe that the superconducting temperature  $T_c$  obtained by the Allen-Dynes formalism is largely affected by correlation effects. In particular, we compare (i) PBE density functional theory, (ii) DFT with many-body corrections obtained by one-shot dynamical mean-field theory (DFT+DMFT), and (iii) DFT+DMFT with the fully charge self-consistent formalism (DFT+DMFT+CSC). We used the typical Koster-Slater interaction vertex for the Ce correlated manifold, with typical values for Ce ( $U = 6$  eV,  $J = 0.6$  eV). As the Hund's coupling controls the splitting of the unoccupied Ce *f*-state spectral features into magnetic multiplets, we provide in Fig. 1 the dependence of  $T_c$  on  $J$ . Interestingly, the one-shot DMFT provides a large increase in the superconducting temperature [see Fig. 1(a)], largely overshooting the experimental value  $T_c = 130$  K, which is concomitant with a sizable increase in  $\log(\omega)$ . The charge self-consistency mitigates this effect [ $\log(\omega)$  remains in line with the PBE value] and in turn reduces the  $T_c$ . This confirms that many-body effects have a sizable contribution to the calculation of the superconducting temperatures in lanthanide hydrides. Note that we use  $J = 0.6$  eV throughout the rest of this paper.

Although DMFT readily provides important corrections to the electronic character, it is worthwhile to explore its effect on the structural properties. As the computational overhead to perform many-body corrections remains significant,

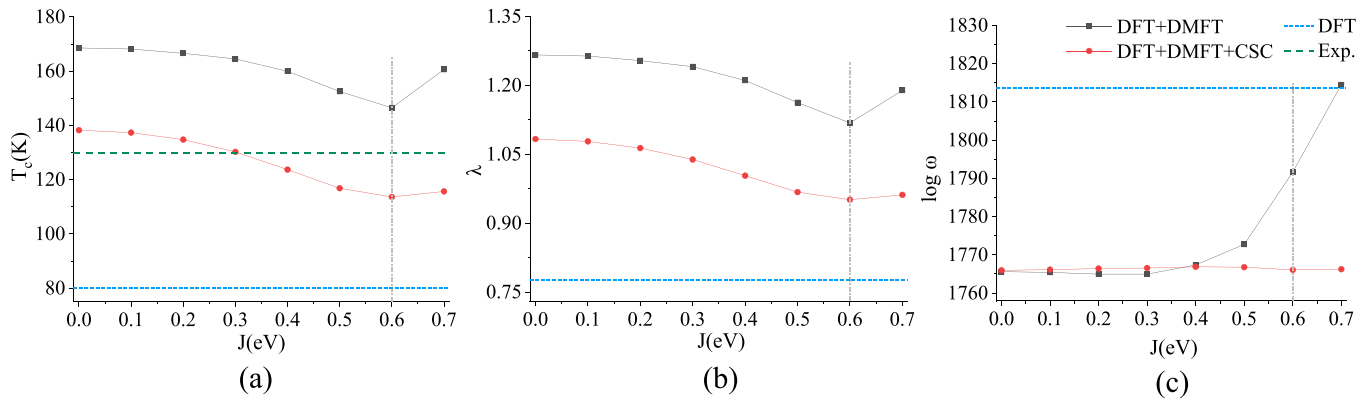


FIG. 1. Many-body corrections to the superconducting temperature. We report (a) the superconducting temperature  $T_c$  obtained by the Allen-Dynes formalism, (b) the electron-phonon coupling strength  $\lambda$ , and (c)  $\log(\omega)$ , as a function of the Hund's coupling  $J$ . The spectral weight at the Fermi level is obtained at different levels of approximation: (i) PBE density functional theory (horizontal light blue short-dashed line), (ii) DFT with many-body corrections obtained by one-shot dynamical mean-field theory (DFT+DMFT, filled black squares), and (iii) DFT+DMFT with the fully charge self-consistent formalism (DFT+DMFT+CSC, filled red circles). The many-body corrections systematically improve the DFT  $T_c$  in the direction of the experimental value (horizontal long-dashed line). The one-shot DMFT provides a large increase in the superconducting temperature, overshooting largely the experimental value, which is concomitant with a sizable increase in  $\log(\omega)$ . The charge self-consistency mitigates this effect [ $\log(\omega)$  remains in line with the PBE value] and in turn reduces the  $T_c$ . The physical value of the Hund's coupling for Ce ( $J \approx 0.6$  eV) is reported by the vertical dash-dotted line in all panels. All calculations were performed in the  $P6_3/mmc$  phase of  $CeH_9$  at 200 GPa.

calculating forces with finite atomic displacement is not tractable. Recent progress has, however, been made in this direction [22], in particular, with the generalization of the Hellmann-Feynman theorem for DMFT in the presence of ultrasoft pseudopotentials [21] in CASTEP [23]. This generalization opens new avenues for systems with heavy elements, not well suited for all-electron calculations. We report in Fig. 2 the structural relaxation at 200 GPa. We typically obtain corrections for the bond lengths of order 4%. As expected, many-body effects tend to increase the length of Ce-H bonds, associated with a reduction in the hybridization induced by electronic correlations. This bond length increase is also concomitant with a small increase in the minimum H-H distance. The volumetric density is also weakly affected by many-body effects, as the pressure obtained from DFT+DMFT+CSC calculations on the DFT structure yields 216 GPa. We hence conclude that DFT is a reasonable approximation for the structural properties of  $CeH_9$ .

The lattice dynamics for  $CeH_9$  (see Fig. 3) leads to a typical phonon gap for lanthanide clathrates (between approximately 300 and 750  $\text{cm}^{-1}$ ) and high frequency modes dominated by hydrogen character ( $\approx 750\text{--}2000$   $\text{cm}^{-1}$ ). The latter leads to a large weight in the Eliashberg function between 0.1 and 0.25 eV, i.e., in the region that mostly contributes to the electron-phonon coupling strength  $\lambda$ . The effect of many-body corrections is indicated in Fig. 3(b), with an increase in the latter energy region due to the DMFT corrections [the trend follows the one observed in Fig. 1(a)].

The changes highlighted above stem directly from a spectral weight transfer induced by many-body corrections [see Fig. 4(a)]. In DFT, the Ce system is described by a two-band system in the absence of long-range magnetic order. We note that DFT is a single-Slater-determinant approach and hence cannot capture the role of paramagnetism, with an associated magnetic multiplet (fluctuating magnetic moment). Such

effects typically induce a splitting of spectral features into satellites, as observed in Figs. 4(b) and 4(c), with a resulting

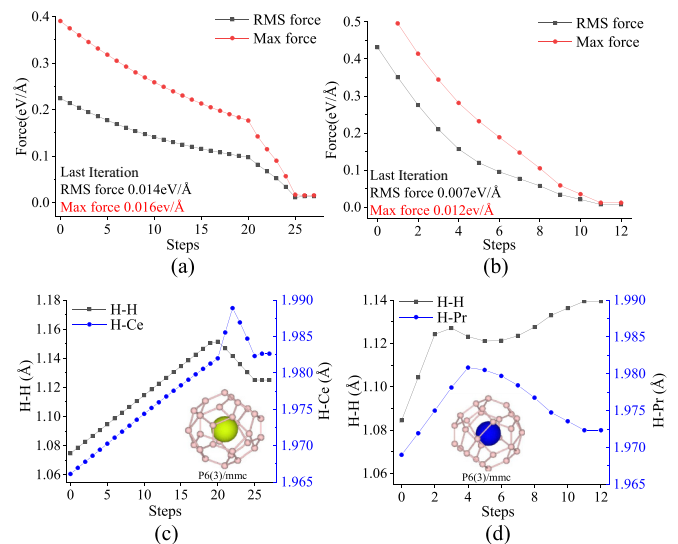


FIG. 2. Structural relaxation of clathrate lanthanides with many-body corrections. We report the structural relaxation of the  $CeH_9$  [(a) and (c)] and prototype  $PrH_9$  [(b) and (d)] compounds. All calculations are performed at 200 GPa. The volume density is obtained by the equation of state in DFT+DMFT+CSC, which provides very similar results to PBE (not shown). Internal coordinates are relaxed with DFT+DMFT+CSC, building upon the recent implementation of DFT forces for ultrasoft pseudopotentials [21]. We report the forces and total energies obtained during the structural optimization, respectively, in (a) [in (b)] for  $CeH_9$  ( $PrH_9$ ). Convergence is obtained within 25 iterations. The shortest H-H and Ce-H bond lengths increase throughout the structural optimization [see (c) and (d) for Ce and Pr hydrides, respectively].

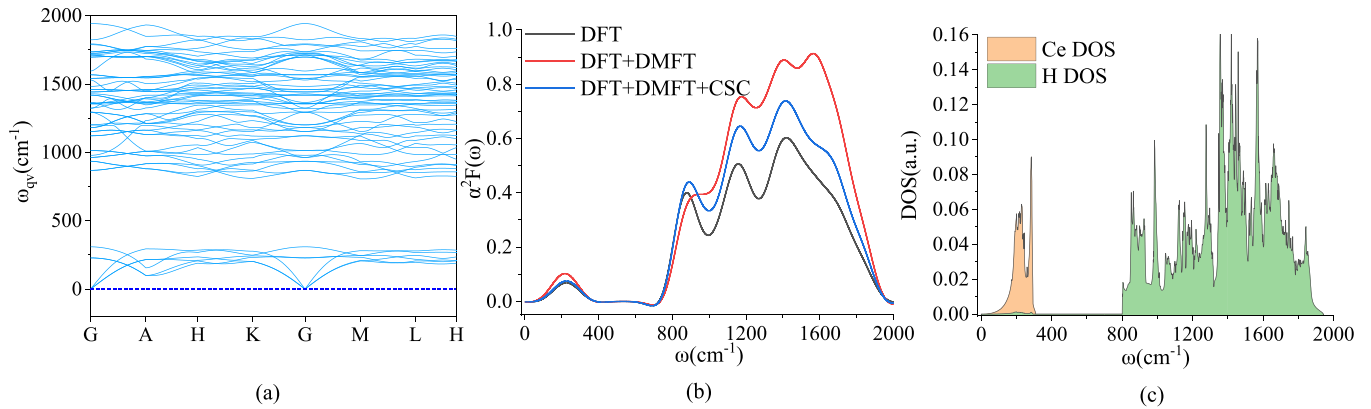


FIG. 3. Lattice dynamics of  $\text{CeH}_9$  at high pressure. (a) Phonon-dispersion relation, (b) Eliashberg function  $\alpha^2F(\omega)$ , and (c) phonon density of states for the  $P6_3/mmc$  phase of  $\text{CeH}_9$  at 200 GPa. The phonon density of states is resolved in the Ce and H contributions. The dominant contribution to the Eliashberg function is due to the hydrogen vibrational modes located above the phonon gap ( $\omega > 750 \text{ cm}^{-1}$ ).

large increase in  $f$  character at the Fermi level. As sharp Ce features occur near the Fermi level, we emphasize that a high level of theory is required to capture correctly the superconducting properties. For instance, in our calculations the fully charge self-consistent approach (DFT+DMFT+CSC) induces a small shift of the sharp Ce feature at the Fermi level, which in turn mitigates the  $f$  character increase at the Fermi level.

As the role of  $f$  electronic orbitals is paramount for the superconducting properties, we study a prototype lanthanide

clathrate with higher  $f$  occupations, by considering the aliovalent praseodymium hydride  $\text{PrH}_9$ . We note that this system is only metastable at 200 GPa in experiments [24], although stable in the pressure range 90–140 GPa with a superconducting temperature  $T_c = 55 \text{ K}$  above 110 GPa. We report in Fig. 5 the DFT+DMFT+CSC framework applied to  $\text{PrH}_9$  in the  $P6_3/mmc$  phase at 200 GPa. We obtain a theoretical estimate of  $T_c = 70 \text{ K}$ , in qualitative agreement with the experimental value obtained at lower pressure, where the  $P6_3/mmc$  phase is stable. In line with the  $\text{CeH}_9$  calculations, DFT also underestimates the critical temperature of  $\text{PrH}_9$ , with  $T_c = 12 \text{ K}$  for  $\mu^* = 0.1$ .

We attribute the decrease in  $T_c$  with the higher  $f$  occupation, which shifts the chemical potential away from the  $f$  spectral features present near the Fermi level [see Fig. 5(a)]. As expected, the lattice dynamics [see Fig. 5(b)] are qualitatively similar to those of the  $\text{CeH}_9$  compound.

Our results highlight a pathway for the optimization of  $T_c$  in lanthanide hydrides: The increase in  $f$  character at the Fermi level in DFT+DMFT, associated with a smaller degree of Ce-H covalency and lesser degree of hybridization, provides a marker for an increased superconducting temperature in these systems.

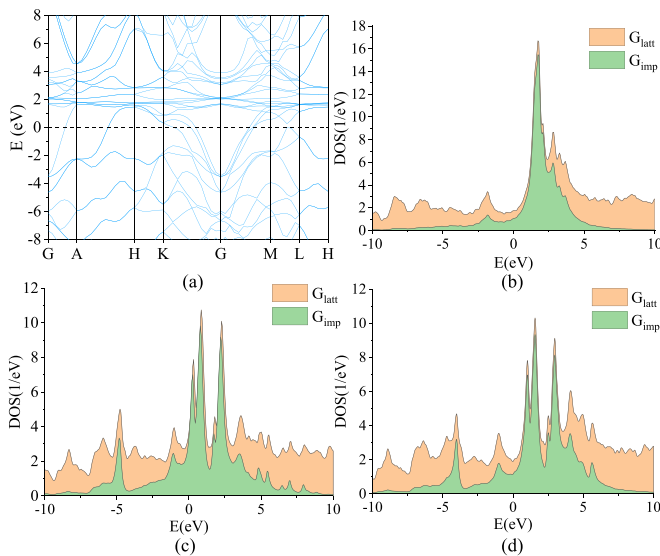


FIG. 4. Spectral weight transfer induced by many-body corrections. (a) Electronic band structure and (b) density of states obtained by DFT calculations.  $G_{\text{latt}}$  and  $G_{\text{imp}}$  denote the spectral weight obtained by the imaginary part of the lattice and  $f$  impurity Green's function, respectively, corresponding to the spectral weight traced over all orbitals and traced over the  $f$  orbitals, respectively. In (c) and (d) we show the energy-resolved spectral weight, obtained by the one-shot DFT+DMFT and the fully charge self-consistent DFT+DMFT+CSC, respectively. All calculations were performed in the  $P6_3/mmc$  phase of  $\text{CeH}_9$  at 200 GPa.

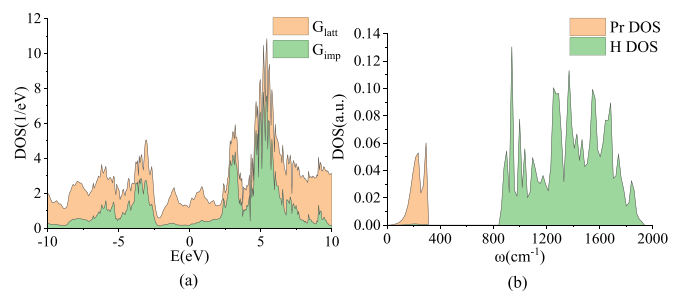


FIG. 5. Aliovalent clathrate Pr prototype. (a) Electronic density of states obtained by DFT+DMFT+CSC and (b) phonon density of states for the  $P6_3/mmc$  phase of  $\text{PrH}_9$  at 200 GPa; the density of states is resolved in the Pr and H contributions. In stark contrast with the  $\text{CeH}_9$  clathrate, the spectral weight of  $f$  electrons is suppressed at the Fermi level, resulting in a lower  $T_c$ .

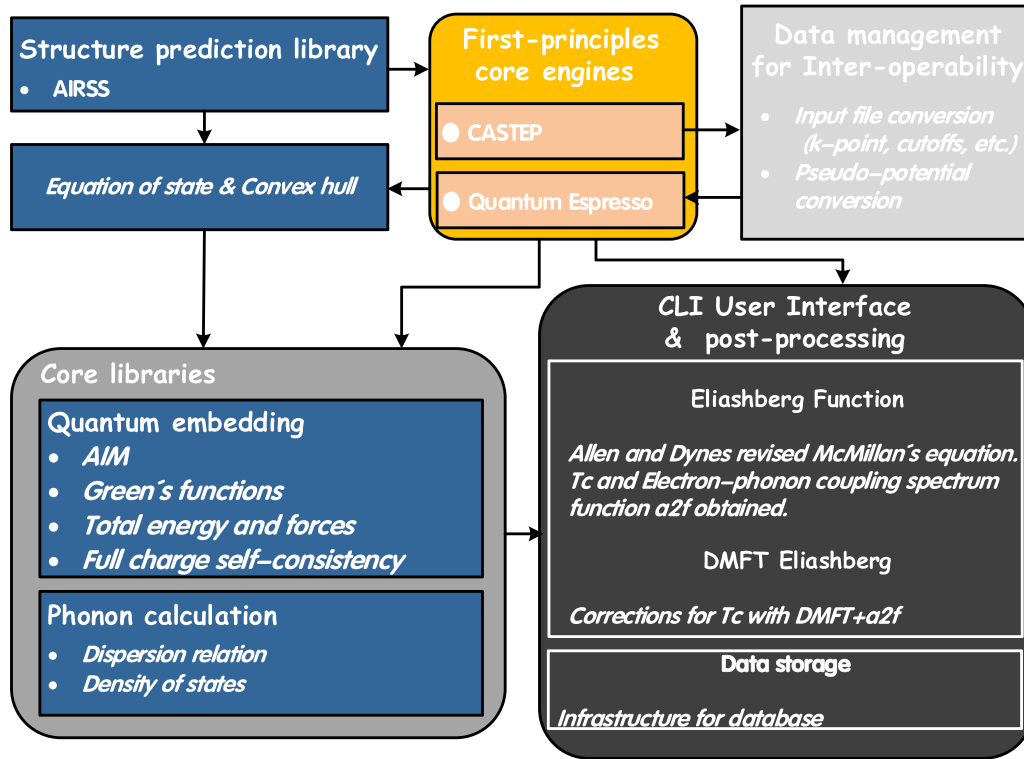


FIG. 6. DFT interoperability for a consistent many-body platform. Schematic overview of the main modules of the theoretical platform and their interrelations. Firstly, structures are predicted by *ab initio* random structure searching (AIRSS), via Gibbs enthalpies for the equation of state and convex hull. The underlying core engines are the CASTEP and QUANTUM ESPRESSO DFT software packages. Interoperability between QE and CASTEP is achieved via format conversion of input files, pseudopotentials, and  $\mathbf{k}$ -point grids. Core libraries are used to provide the many-body corrections, via quantum embedding, which in turn provides corrected forces and energies. In postprocessing, the Eliashberg function and superconducting  $T_c$  are obtained with the DMFT+a2F approach. Finally, data are archived for future usage in hierarchical data format version 5 (hdf5). CLI, command-line interface.

### III. METHODS

We present our theoretical approach in Fig. 6. We report a schematic overview of the main modules of the theoretical platform and their interrelations. Our approach provides a modular framework for systematic material screening at high pressure. Firstly, stoichiometric compositions are provided by *ab initio* random structure searching (AIRSS) [25], via Gibbs enthalpies for the equation of state and convex hull. The underlying core engines are CASTEP [26] and QUANTUM ESPRESSO (QE) [27], both interfaced with AIRSS. Interoperability between QE and CASTEP is achieved via format conversion of input files, pseudopotentials and  $\mathbf{k}$ -point grids. Core libraries are used to provide the many-body corrections, via the DMFT quantum embedding, which in turn provides corrected forces [21] and total energies [23,28].

The underlying structure relaxations were carried out using the QE and CASTEP packages in the framework of DFT and using the Perdew-Burke-Ernzerhof generalized gradient approximation (PBE-GGA) [29,30]. Ultrasoft pseudopotentials were used to describe the core electrons and their effects on valence orbitals. A valence electron configuration of  $5s^25p^64f^15d^16s^2$  (i.e., with explicitly included  $f$  electrons) and  $1s^1$  was used for the Ce and H atoms, respectively. A plane-wave kinetic-energy cutoff of 1000 eV and dense Monkhorst-Pack  $\mathbf{k}$ -point grids with reciprocal space resolution of  $2\pi \times 0.07 \text{ \AA}^{-1}$  were employed in the calculation.

Phonon frequencies and superconducting critical temperature were calculated using density-functional perturbation theory as implemented in QUANTUM ESPRESSO. The  $\mathbf{k}$ -space integration (electrons) was approximated by a summation over a  $24 \times 24 \times 12$  uniform grid in reciprocal space, with the smearing scheme of Methfessel and Paxton using a temperature  $k_B T = 0.05$  eV for self-consistent cycles and relaxations; the same grid ( $24 \times 24 \times 12$ ) was used for evaluating density of states (DOS) and coupling strength. Dynamical matrices and  $\lambda$  were calculated on a uniform  $6 \times 6 \times 3$  grid in  $\mathbf{q}$  space for  $P6_3/mmc$ -CeH<sub>9</sub>.

In postprocessing, the superconducting transition temperature  $T_c$  was estimated using the Allen-Dynes modified McMillan equation:

$$T_c = \frac{\omega_{\log}}{1.2} \exp \left[ \frac{-1.04(1 + \lambda)}{\lambda - \mu^*(1 + 0.62\lambda)} \right], \quad (1)$$

where  $\mu^*$  is the Coulomb pseudopotential. The electron-phonon coupling strength  $\lambda$  and  $\omega_{\log}$  were calculated as

$$\omega_{\log} = \exp \left[ \frac{2}{\lambda} \int \frac{d\omega}{\omega} \alpha^2 F(\omega) \log(\omega) \right], \quad (2)$$

$$\lambda = \sum_{\mathbf{qv}} \lambda_{\mathbf{qv}} = 2 \int \frac{\alpha^2 F(\omega)}{\omega} d\omega. \quad (3)$$

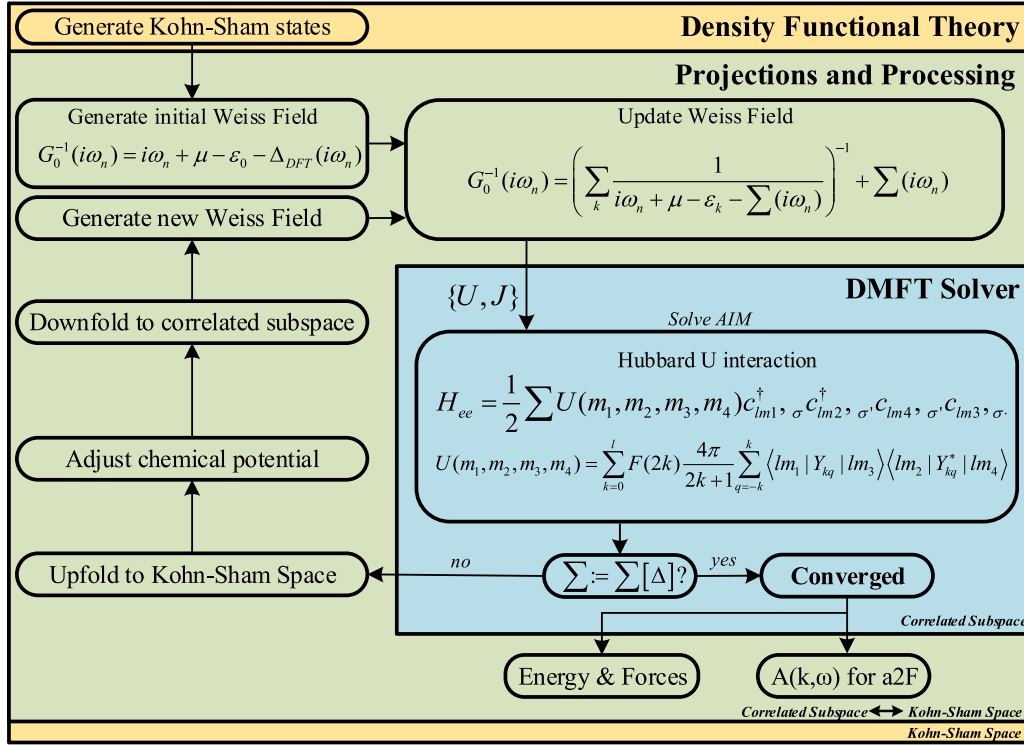


FIG. 7. The fully charge self-consistent DMFT approach. Flowchart of the DFT+DMFT calculations. The outer region denotes the density functional theory, which provides the Kohn-Sham potentials that in turn feed into the calculation of the Green's function (midregion). The projected Green's function provides in turn the Weiss field, which is used to define the Anderson impurity model, solved in the presence of a general two-body correlation term (inner region). In the fully charge self-consistent approach (DFT+DMFT+CSC), the Kohn-Sham potentials are calculated from the DMFT electronic density. Upon DMFT convergence, total energies and forces are calculated from the Green's function and self-energy. The colors separate the procedure by levels of theory: The outer region deals with DFT, the midregion is dealing with the interface between DFT and the AIM, and the inner region is where the AIM is solved by the quantum solver.

In the Allen-Dynes formalism, the Eliashberg function  $\alpha^2 F(\omega)$  is obtained by summing over all scattering processes at the Fermi level mediated by phonon momentum transfer and reads [31]

$$\alpha^2 F(\omega) = N(\epsilon_F) \frac{\sum_{\mathbf{k}_1, \mathbf{k}_2} |M_{\mathbf{k}_1, \mathbf{k}_2}|^2 \delta(\omega - \omega_{\mathbf{q}\nu}) \delta(\epsilon_{\mathbf{k}_1}) \delta(\epsilon_{\mathbf{k}_2})}{\sum_{\mathbf{k}_1, \mathbf{k}_2} \delta(\epsilon_{\mathbf{k}_1}) \delta(\epsilon_{\mathbf{k}_2})}. \quad (4)$$

Here,  $N(\epsilon_F)$  is the DOS at the Fermi level,  $\omega_{\mathbf{q}\nu}$  is the phonon spectrum of a branch  $\nu$  at momentum  $\mathbf{q} = \mathbf{k}_2 - \mathbf{k}_1$ ,  $\epsilon_{\mathbf{k}_1}$  and  $\epsilon_{\mathbf{k}_2}$  are electronic band energies referred to the Fermi level, and  $M_{\mathbf{k}_1, \mathbf{k}_2}$  are the electron-phonon coupling matrix elements. Many-body effects introduce a change of spectral character at the Fermi level, where electronic correlations induce a mass enhancement and introduce a finite lifetime, due to incoherence. In this spirit of the DMFT scissors [32], we correct the DFT bands with the renormalized DMFT band picture:

$$\alpha^2 F(\omega) = \mathcal{A}_{\text{tot}} \frac{\sum_{\mathbf{k}_1, \mathbf{k}_2} |M_{\mathbf{k}_1, \mathbf{k}_2}|^2 \delta(\omega - \omega_{\mathbf{q}\nu}) \mathcal{A}(\mathbf{k}_1) \mathcal{A}(\mathbf{k}_2)}{\sum_{\mathbf{k}_1, \mathbf{k}_2} \mathcal{A}(\mathbf{k}_1) \mathcal{A}(\mathbf{k}_2)}, \quad (5)$$

where  $\mathcal{A}_{\text{tot}}$  and  $\mathcal{A}(\mathbf{k})$  are the total and  $\mathbf{k}$ -momentum-resolved spectral weights, respectively, at the Fermi level. This approach is denoted as *DMFT+a2F* in the workflow.

Figure 7 indicates the DMFT quantum embedding approach. Density functional theory provides the Kohn-Sham Hamiltonian that in turn feeds into the calculation of the DMFT Green's function. We use atomic projectors to define the Anderson impurity model (AIM), solved with a Hubbard-I solver. A breadth of quantum solvers are readily available in the Toolbox for Research on Interacting Quantum Systems (TRIQS) open-source platform [33,34]. In the fully charge self-consistent approach (DFT+DMFT+CSC), the Kohn-Sham potentials are calculated from the DMFT electronic density, obtained by the trace of the Green's function [23]. Upon DMFT convergence, total energies and forces are calculated from the Green's function and self-energy. All DFT calculations carried out in this paper are with pseudopotentials. To validate the latter approach, we have benchmarked the pseudopotential calculations with all-electron calculations done with QUESTAAL, as documented [35] (see Fig. 8).

#### IV. CONCLUSION

We have developed a framework that can readily provide many-body corrections to the estimation of the superconducting temperature in lanthanide hydrides. We observe sizable corrections to the uncorrected first-principles calculation when keeping in account many-body effects, and recover consistent agreement with experiments for CeH<sub>9</sub> at 200 GPa. We report that the DMFT charge self-consistency, i.e., the

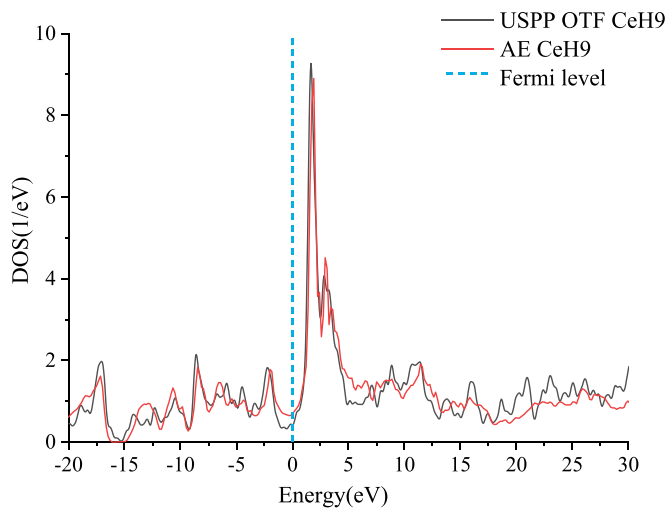


FIG. 8. Benchmark of pseudopotentials. To assess the validity of the choice of pseudopotentials in the workflow, we have carried out a calculation with QUESTAAL at 200 GPa for CeH<sub>9</sub>, within the linear muffin-tin approximation. The results indicate an excellent agreement, for semicore, valence, and conduction states (up to 30 eV). AE, all-electron calculation; OTF USPP, On the Fly UltraSoft Pseudopotential generated by CASTEP.

many-body corrections to the local charge density in the first-principles calculations, is instrumental to recover a consistent theoretical framework. The increase in the calculated superconducting temperature is induced by a shift of the spectral weight of the  $f$  states, which in turn affects the spectral character at the Fermi level. Albeit hitherto the many-body corrections remain limited to the electronic contribution to the Eliashberg function, we have discussed the capabilities for relaxing lanthanide hydrides within the DMFT formalism, building upon our recent developments that provide DMFT

forces for DFT with norm-conserving and ultrasoft pseudopotential. The latter provides structural insights, and we report that at large pressure many-body effects have small effects on the lattice, as DFT structures and pressures are close to the DMFT counterparts. Although a full treatment of phonons at the DMFT level remains out of reach for such complex materials, the latter suggests that the largest corrections to  $T_c$  lie with many-body corrections to the electronic part. We have studied the aliovalent effect and observed that the increase in  $f$  character at the Fermi level, as compared with an isostructural Pr hydride, leads to an increase in superconducting temperature, a compelling observation for future explorations of  $f$  systems as high  $T_c$  superconductors. Our approach is general and provides a modular framework to interoperate typical first-principles software, i.e., the freely available CASTEP+DMFT code and QUANTUM ESPRESSO, with a relatively small numerical footprint and is straightforward to implement.

The codes are available [36] under the GPL 3.0 license.

#### ACKNOWLEDGMENTS

C.W., N.B., and E.P. are supported by Grant No. EP/R02992X/1 from the UK Engineering and Physical Sciences Research Council (EPSRC). This work was performed using resources provided by the ARCHER UK National Supercomputing Service and the Cambridge Service for Data Driven Discovery (CSD3) operated by the University of Cambridge Research Computing Service [37], provided by Dell EMC and Intel using Tier-2 funding from the Engineering and Physical Sciences Research Council (Capital Grant No. EP/P020259/1) and DiRAC funding from the Science and Technology Facilities Council [38].

Z.Z., F.M., Y.W., and E.P. carried out the calculations. All authors wrote the paper. C.W. designed the research.

- [1] J. S. Schilling, The use of high pressure in basic, materials, and life sciences, *Hyperfine Interact.* **128**, 3 (2000).
- [2] T. Matsuoka and K. Shimizu, Direct observation of a pressure-induced metal-to-semiconductor transition in lithium, *Nature (London)* **458**, 186 (2009).
- [3] M. I. McMahon, R. J. Nelmes, U. Schwarz, and K. Syassen, Composite incommensurate K-III and a commensurate form: Study of a high-pressure phase of potassium, *Phys. Rev. B* **74**, 140102(R) (2006).
- [4] C. L. Guillaume, E. Gregoryanz, O. Degtyareva, M. I. McMahon, M. Hanfland, S. Evans, M. Guthrie, S. V. Sinogeikin, and H. Mao, Cold melting and solid structures of dense lithium, *Nat. Phys.* **7**, 211 (2011).
- [5] N. W. Ashcroft, Hydrogen Dominant Metallic Alloys: High Temperature Superconductors? *Phys. Rev. Lett.* **92**, 187002 (2004).
- [6] M. I. Eremets, I. A. Trojan, S. A. Medvedev, J. S. Tse, and Y. Yao, Superconductivity in hydrogen dominant materials: Silane, *Science* **319**, 1506 (2008).
- [7] A. Drozdov, M. Eremets, I. Troyan, V. Ksenofontov, and S. I. Shylin, Conventional superconductivity at 203 kelvin at high pressures in the sulfur hydride system, *Nature (London)* **525**, 73 (2015).
- [8] E. Snider, N. Dasenbrock-Gammon, R. McBride, M. Debessai, H. Vindana, K. Vencatasamy, K. V. Lawler, A. Salamat, and R. P. Dias, Room-temperature superconductivity in a carbonaceous sulfur hydride, *Nature (London)* **586**, 373 (2020).
- [9] Y. Li, J. Hao, H. Liu, Y. Li, and Y. Ma, The metallization and superconductivity of dense hydrogen sulfide, *J. Chem. Phys.* **140**, 174712 (2014).
- [10] M. Einaga, M. Sakata, T. Ishikawa, K. Shimizu, M. I. Eremets, A. P. Drozdov, I. A. Troyan, N. Hirao, and Y. Ohishi, Crystal structure of the superconducting phase of sulfur hydride, *Nat. Phys.* **12**, 835 (2016).
- [11] M. Kostrzewa, K. Szczęśniak, A. Durajski, and R. Szczęśniak, From LaH<sub>10</sub> to room-temperature superconductors, *Sci. Rep.* **10**, 1592 (2020).
- [12] H. Li, I. I. Naumov, R. Hoffmann, N. Ashcroft, and R. J. Hemley, Potential high- $T_c$  superconducting lanthanum and yttrium hydrides at high pressure, *Proc. Natl. Acad. Sci. USA* **114**, 6990 (2017).

- [13] Y. Li, J. Hao, H. Liu, J. S. Tse, Y. Wang, and Y. Ma, Pressure-stabilized superconductive yttrium hydrides, *Sci. Rep.* **5**, 9948 (2015).
- [14] J. Zaanen, G. A. Sawatzky, and J. W. Allen, Band Gaps and Electronic Structure of Transition-Metal Compounds, *Phys. Rev. Lett.* **55**, 418 (1985).
- [15] C. P. Koçer, K. Haule, G. L. Pascut, and B. Monserrat, Efficient lattice dynamics calculations for correlated materials with DFT + DMFT, *Phys. Rev. B* **102**, 245104 (2020).
- [16] J. Kolorenč, Metal-oxygen hybridization and core-level spectra in actinide and rare-earth oxides, *MRS Adv.* **1**, 3007 (2016).
- [17] R. Sakuma, T. Miyake, and F. Aryasetiawan, Self-energy and spectral function of Ce within the *GW* approximation, *Phys. Rev. B* **86**, 245126 (2012).
- [18] N. Devaux, M. Casula, F. Decremps, and S. Sorella, Electronic origin of the volume collapse in cerium, *Phys. Rev. B* **91**, 081101(R) (2015).
- [19] A. Drozdov, P. P. Kong, V. S. Minkov, S. P. Besedin, M. A. Kuzovnikov, S. Mozaffari, L. Balicas, F. F. Balakirev, D. E. Graf, V. B. Prakapenka, E. Greenberg, D. A. Knyazev, M. Tkacz, and M. I. Eremets, Superconductivity at 250 K in lanthanum hydride under high pressures, *Nature (London)* **569**, 528 (2019).
- [20] N. P. Salke, M. M. Davari Esfahani, Y. Zhang, I. A. Kruglov, J. Zhou, Y. Wang, E. Greenberg, V. B. Prakapenka, J. Liu, A. R. Oganov, and J.-F. Lin, Synthesis of clathrate cerium superhydride CeH<sub>9</sub> at 80–100 GPa with atomic hydrogen sublattice, *Nat. Commun.* **10**, 4453 (2019).
- [21] E. Plekhanov, N. Bonini, and C. Weber, Calculating dynamical mean-field theory forces in *ab initio* ultrasoft pseudopotential formalism, *Phys. Rev. B* **104**, 235131 (2021); Y. Wei, F. Macheda, Z. Zhao, T. Tse, E. Plekhanov, N. Bonini, and C. Weber, High-temperature superconductivity in the lanthanide hydrides at extreme pressures, *Appl. Sci.* **12**, 874 (2022).
- [22] K. Haule and G. L. Pascut, Forces for structural optimizations in correlated materials within a DFT+embedded DMFT functional approach, *Phys. Rev. B* **94**, 195146 (2016).
- [23] E. Plekhanov, P. Hasnip, V. Sacksteder, M. Probert, S. J. Clark, K. Refson, and C. Weber, Many-body renormalization of forces in *f*-electron materials, *Phys. Rev. B* **98**, 075129 (2018).
- [24] D. Zhou, D. V. Semenok, D. Duan, H. Xie, W. Chen, X. Huang, X. Li, B. Liu, A. R. Oganov, and T. Cui, Superconducting praseodymium superhydrides, *Sci. Adv.* **6**, eaax6849 (2020).
- [25] C. J. Pickard and R. J. Needs, *Ab initio* random structure searching, *J. Phys.: Condens. Matter* **23**, 053201 (2011).
- [26] S. J. Clark, M. D. Segall, C. J. Pickard, P. J. Hasnip, M. J. Probert, K. Refson, and M. Payne, First principles methods using CASTEP, *Z. Kristallogr.* **220**, 567 (2005).
- [27] P. Giannozzi, S. Baroni, N. Bonini, M. Calandra, R. Car, C. Cavazzoni, D. Ceresoli, G. L. Chiarotti, M. Cococcioni, I. Dabo, A. D. Corso, S. de Gironcoli, S. Fabris, G. Fratesi, R. Gebauer, U. Gerstmann, C. Gougoussis, A. Kokalj, M. Lazzeri, L. Martin-Samos *et al.*, QUANTUM ESPRESSO: A modular and open-source software project for quantum simulations of materials, *J. Phys.: Condens. Matter* **21**, 395502 (2009).
- [28] H. Lee, E. Plekhanov, D. Blackbourn, S. Acharya, and C. Weber, The Mott to Kondo transition in diluted Kondo superlattices, *Commun. Phys.* **2**, 49 (2019).
- [29] J. P. Perdew, J. A. Chevary, S. H. Vosko, K. A. Jackson, M. R. Pederson, D. J. Singh, and C. Fiolhais, Atoms, molecules, solids, and surfaces: Applications of the generalized gradient approximation for exchange and correlation, *Phys. Rev. B* **46**, 6671 (1992).
- [30] J. P. Perdew, K. Burke, and M. Ernzerhof, Generalized Gradient Approximation Made Simple, *Phys. Rev. Lett.* **77**, 3865 (1996).
- [31] P. B. Allen and R. C. Dynes, Transition temperature of strong-coupled superconductors reanalyzed, *Phys. Rev. B* **12**, 905 (1975).
- [32] J. M. Tomczak and S. Biermann, Effective band structure of correlated materials: The case of VO<sub>2</sub>, *J. Phys.: Condens. Matter* **19**, 365206 (2007).
- [33] M. Aichhorn, L. Pourovskii, P. Seth, V. Vildosola, M. Zingl, O. E. Peil, X. Deng, J. Mravlje, G. J. Kraberger, C. Martins, M. Ferrero, and O. Parcollet, TRIQS/DFTTools: A TRIQS application for *ab initio* calculations of correlated materials, *Comput. Phys. Commun.* **204**, 200 (2016).
- [34] P. Seth, I. Krivenko, M. Ferrero, and O. Parcollet, TRIQS/CTHYB: A continuous-time quantum Monte Carlo hybridisation expansion solver for quantum impurity problems, *Comput. Phys. Commun.* **200**, 274 (2016).
- [35] <https://www.questaal.org>.
- [36] <https://nms.kcl.ac.uk/cedric.weber/>.
- [37] <https://www.hpc.cam.ac.uk/>.
- [38] <https://www.dirac.ac.uk>.